14. Fundamentals of Monte Carlo particle transport and synergies with quantum dynamics for applications in ion-irradiated materials in Space and radiobiology

Fabiana Da Pieve[*]*, Natalia Koval, Bin Gu, Daniel Muñoz-Santiburcio, Johannes Teunissen, Emilio Artacho, Jorge Kohanoff, and Fabrizio Cleri*

First-stage radiation effects induced in detectors in accelerators, electronic devices and solar arrays in space, shielding materials for spacecraft, materials in nuclear power plants, and in water samples as proxies for biological matter are traditionally studied via Monte Carlo particle transport approaches. In this chapter, we introduce the basic notions of Monte Carlo particle transport and some of the practicalities of the related codes, also mentioning the low energy extension specific to the case of radiation effects in biological matter. Then, we will discuss some applications in the studies of radiation effects in space and planetary missions and in radiobiology, where synergistic studies between the Monte Carlo community and the condensed matter/chemical-physics community are possible.

[*] Contact: fabiana.dapieve@gmail.com

14.1 Introduction

The study of radiation-induced effects on materials and biological systems is of importance for several fields of science, including the study of the damage of detectors in high energy particle physics experiments, the performance of materials in reactors, the damage of spacecraft components, the biological risks in missions to Space and ion-beam cancer therapy. In many applications, the primary radiation to be investigated are hadrons (such as protons), neutrons or heavy ions; such primary particles produce secondaries, which include other hadrons, electrons and photons. For all these particles (including high-energy photons, treated as quantum-mechanical particles) the associated interactions must be taken into account, with different degrees of detail according to the required accuracy of the simulation.

Given the high number of generated particles through the medium and the high number of scattering integrals (related to different interactions the primary and secondary particles can have, in different energy ranges), the early-stage radiation effects for the above mentioned applications are traditionally studied via Monte Carlo (MC) radiation transport methods, in which a stochastic approach, based on an approximation to the Boltzmann transport equation, is used to simulate the statistically averaged trajectories of model particles as they travel across the matter.

In the following, after a brief summary of the fundamentals of charged particles interactions with matter in a large energy range, we illustrate the fundamental notions of MC particle transport [1,2,3,4], in both the so-called condensed history approach suitable for high energy applications and in the track structure approach for the study of radiation effects in biological targets at the micro- and nanoscale. We then present some technicalities of the MC calculations and in the end we make a brief excursion in the applications related to radiation-induced effects in spacecraft components, in water/icy targets of interest for planetary exploration, and in radiobiology. In particular, we will focus on possible synergies between the first-principles chemical-physics/condensed matter approaches and the MC particle transport approaches, for problems related to radiation-induced effects by those interactions (among the many considered in MC approaches used in the applications mentioned above) occurring in the low-energy regime. While in MC approaches there is actually no real dynamics of the systems, coupled electron-nuclear dynamics in TDDFT [5] and ab-initio Molecular Dynamics (MD) [6] allow to study the dynamical response of the system and can provide insights into the quantities provided by MC codes, ameliorate some input datasets used by the latter in the low energy regime and clarify the accuracy of internationally recommended datasets commonly used to benchmark MC results.

14.1.1 Brief summary of interactions

In many applications, the transport of protons and other charged particles is of relevance. The number of interactions these can have with matter is daunting, and cross sections are based, depending on the energy range, either on experimental data, or on sole (not parameter-free) models or on parameterized models which extend reduced set of experimental data to larger energy windows. Differently from Chapter 7, we will mention here not only the interactions that the incoming particle can have with the electrons in the target material, but also the other interactions that a particle in high energy applications can induce in the system. The main classes of interactions for protons and charged hadrons are:

- electronic interactions with electrons, such as ionization/excitations, described through the electronic stopping power;
- multiple Coulomb scattering at small angles (elastic deflection without energy loss, or very small inelastic loss);
- inelastic nuclear reactions (>30-50 MeV): these are high-energy nuclear reactions in which a target nucleus struck by an incident particle (*p+, n, π,* etc.) of energy typically above a few tens MeV, can lead to fragmentation into secondary lighter nuclei and/or lighter particles. Such nuclear reactions are considered to take place in two steps:
  1) a fast direct stage intranuclear cascade (~10^{-22} sec), where the incident proton/ion knocks out several nucleons; At low projectile energies (<100 MeV), all interactions occur just between nucleons and the process is called nucleon cascade [7]. With increasing energy, firstly pions come out (at energies of about hundreds of MeV), then at higher energies (~ 2 – 10 GeV) heavier hadrons are produced. These heavier particles can also participate in the intra-nuclear cascade and interact between each other, in what is called a hadron cascade. Particles that gain high enough energy to escape from the nucleus are emitted mainly in the direction of the incident particle; the rest of the energy is distributed in the nucleus, which is left in a highly excited state. In the intranuclear cascade collisions are treated as a series of two-body collisions [8,9,10] or via Quantum Molecular Dynamics models [11], where the reaction is treated in a semi-classical many-body framework, dealing with all correlations among the ejects;
  2) an "evaporation" phase [12] in which the excited nucleus decays by the evaporation of charged particles and neutrons, forming a continuous distribution of products [Figure 14.1]. The evaporated fragments have energies up to ~40 MeV. In this phase, residual particles are emitted in isotropic manner; the reaction yields show different regions according to the different reaction pathways (spallation, fission, fragmentation);
- elastic nuclear interactions (<10-20 MeV): unlike the small angle scattering events at the previous point, the scattering taking place in an elastic nuclear collision is not a glancing one. After penetrating the electron cloud of the target atom, the proton interacts with an unscreened nucleus. Elastic scattering is generally modelled as a hard-sphere collision. In a crystal lattice, atoms are displaced from their initial positions, creating vacancies and interstitials. If the recoil energy of the primary knock-on nucleus is higher than the threshold for atomic displacement, it can produce displacement of a further nucleus, initiating a collisional displacement cascade. Although qualitatively similar, the displacement cross sections for protons are generally larger than those of neutrons, because of the electromagnetic interaction, and pions, because of the larger mass, for a given material (see e.g. [13]); all cross sections rapidly decrease above a few tens of MeV in any material.

Neutrons, being neutral particles, cannot ionize materials. Apart from the inelastic, two-step collisions described above, reactions that may occur in a target under neutron impact are elastic scattering and inelastic scattering with neutron-capture. Elastic scattering is a collision between the neutron and the nucleus, where after reaction, the neutron is deviated from its trajectory with a transfer of kinetic energy and the nucleus is left in the ground state. For inelastic interaction, a neutron is captured by the nucleus and then re-emitted with different energy and momentum (a (*n,n'*) reaction). The resulting nucleus, in an excited state, can de-excite by emission of a *γ*-ray,

charged particles, or other neutrons. For neutrons with energy below 0.5 MeV, the probability of neutron capture increases [2]: the neutron is absorbed by the nucleus, usually accompanied by a γ-ray (the (n, γ) radiative capture).

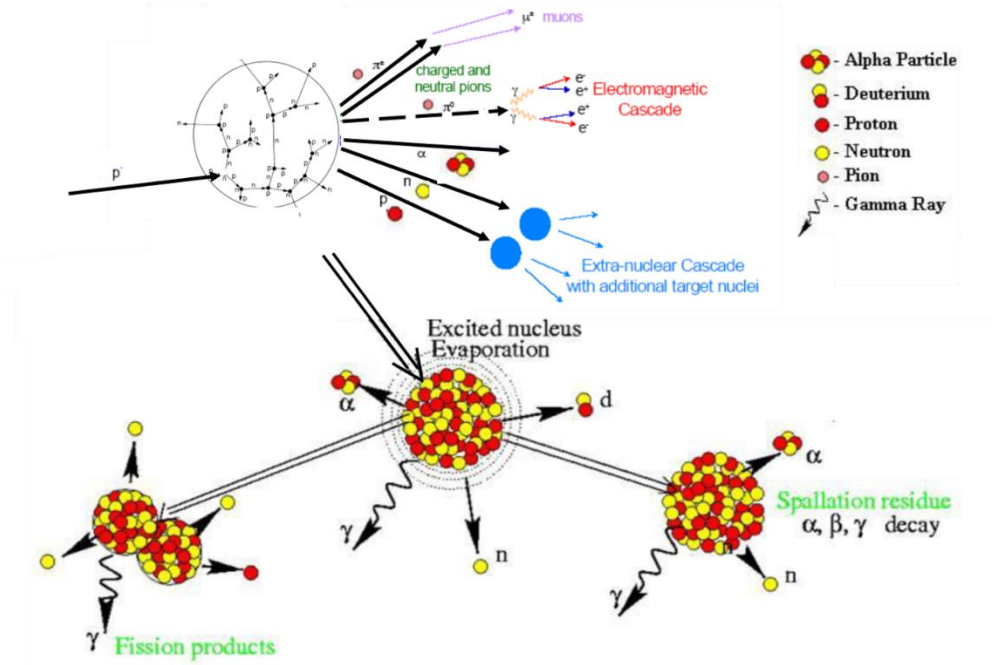

Figure 14.1. Schematic example of a high-energy proton interaction with a heavy target nucleus, and some typical outcomes of the subsequent particle cascade. Adapted from [14] and [15].

Electrons constitute the predominant secondary particle species generated as charged particles traverse matter. Elastic interactions are those in which either the electron passes straight through the sample, or is deflected from its path by Coulomb interaction with the positive potential inside the electron atomic cloud, with no or negligible energy loss. The closer the electron comes to the nucleus, the larger is the scattering angle. The backscattering probability is peaked at energies of 1-10 KeV and rapidly decreases, and gets larger the larger the atomic number Z of the target.

In inelastic electron interactions, the energy transferred to the target can cause emission of secondary electrons. These can be Auger electrons, or other electrons emitted with low energies from the valence states, and with smaller probability higher energy electrons, also called δ-rays, with energies of several hundred keV. Collective excitations such as plasmons, phonons, … can also be induced. Also, an electron passing an atom within its electron cloud is decelerated by the Coulomb force of the nucleus; this inelastic interaction generates a continuous spectrum of high-energy X-rays, with maximum energy equal to that of the incident beam, the *Bremsstrahlung* emission.

At electromagnetic field energies $E=hc/\lambda$ for which the wavelength λ becomes comparable with the atomic size, that is a few keV, the photons can be practically considered as particles with zero mass and momentum $p=E/c$. They can interact with matter through: a) the photoelectric effect; b) Compton scattering, where the photon transfers part of its energy to an atomic electron that is emitted with well defined energy and momentum; c) coherent (Rayleigh) scattering from the atomic electron cloud, with a relatively small contribution for keV energies where the

photoelectric dominates, and negligible for MeV energies; d) positron-electron pair production when the energy of the photon reaches twice the rest energy of an electron (1.022 MeV), and rapidly increasing with increasing photon energy. The positron-electron pair share the excess photon energy (above 1.022 MeV) as kinetic energy. After coming to rest, the positron annihilates with an atomic electron, and a pair of annihilation photons with an energy of 0.511 MeV is produced.

14.2 The Boltzmann equation

When the incoming particle beam is very intense, it becomes meaningless to follow each primary particle individually, and to track all the huge shower of its secondary particles. Instead, a statistical approach is sought, centred on the fundamental notions of phase space and of particle distributions (in position, energy, angle, momentum, time) in the phase space. Each particle *i* is represented by a point with 6 coordinates in phase space, each phase space coordinate corresponding to one of the degrees of freedom of the particle: three correspond to the position *{x,y,z}* and the other three to the vector components of the particle kinetic momentum $\{p_x,p_y,p_z\}$ (also expressed as the triplet of energy and two direction angles, {E,ϑ,ϕ}); if required, spin, particle type, etc. may be considered by adding additional degrees of freedom.

The aim is thus to determine the expected number of particles in a phase space element ($d^3r\,d^3p$) at time *t*, that is the probability density $\mathrm{F} = \mathrm{F}(\vec{r}_i, \vec{p}_i, t), i \in N$, which requires to follow the 6 phase-space coordinates of a macroscopic number of particles *N*, of the order of Avogadro's number. The most accurate, though approximate, equation that describes particle transport in terms of the phase space density is the Boltzmann transport equation, that is obtained from the full equation for the density distribution (the Liouville equation) by rewriting the equation for one representative particle, called the 1-particle density distribution *f*, and averaging over the ensemble of the other particles. By following the time evolution of the 1-particle density $f = f(\vec{r},\vec{p},t) = f(\vec{r},E,\vec{\Omega},t)$ (where $\vec{\Omega}$ is the unitary vector defined by ϑ,ϕ), a complete "history" of the radiation tracks can be obtained (that is, an average space-time distribution of the expected energy-momentum behaviour of the particle beam, transported and scattered across the target).

The Boltzmann equation is an integro-differential non-homogeneous equation, based on the principle of detailed balance in phase space: at any phase space point, the time derivative of *f* is the sum of a contribution from all the particles that arrive at the point $\vec{r}$ with momentum $\vec{p}$ in absence of collisions ("streaming" or free-flight term), plus a contribution from all the particles that arrive at $\vec{r}$ by changing their momentum $\vec{p}' \rightarrow \vec{p}$ as a result of an interaction ("collision" term). In practice, the Boltzmann equation is often written in terms of the particle flux

$$\psi(\vec{r},E,\vec{\Omega},t) = |\vec{v}| \cdot f(\vec{r},E,\vec{\Omega},t) \tag{14.1}$$

with units of [particles]/([surface][time]) [16]:

$$\underbrace{\frac{1}{v}\frac{\partial\psi(x)}{\partial t}}_{time-dependent} + \underbrace{\vec{\Omega}\nabla\psi(x)}_{translation} + \underbrace{\mu_t\psi(x)}_{absorption} - \underbrace{S(x)}_{source} = \underbrace{\int_\Omega\int_E \psi(x)\mu_s(x'\rightarrow x)dx'}_{scattering} \tag{14.2}$$

where *x* represents all phase-space coordinates $\{\vec{r}, \vec{\Omega}, E, t\}$ and $\psi(x)$ is thus the flux of particles at $\vec{r}$ moving along the direction $\vec{\Omega}$ with kinetic energy *E* at time *t*. The different terms in the equation have the following physical meaning:

a. the first term, $1/v \ \partial\psi(x)/\partial t$ is the time-dependent flux change, due to particles escaping from the system boundaries, or disappearing by an absorption reaction, or radioactive decay.

b. $\vec{\Omega}\nabla\psi(x)$ and $\mu_t\psi(x)$ are respectively the flux change due to translation without change of energy and direction (free flight) and the absorption term, with $\mu_t\ (\vec{r}, E, t)$ being the total macroscopic absorption cross section integrated over angles (or attenuation coefficient, inverse of the mean free path = $1/\lambda_t = \sigma_t N_A \rho/A$, where λ_t is the mean free path and σ_t the interaction probability per atom/cm^2).

c. $S(x)$ represents the particle source, external (e.g., a particle beam irradiating the target volume) or internal (e.g. neutrons from fission reactions in the volume).

d. the term on the r.h.s. represents the effect of collisions, or scattering (change in particle flux from changes in direction and energy, without a change of particle position); $\mu_s(\vec{r}:\vec{r}', \vec{\Omega}:\vec{\Omega}', E:E', t:t')$ is the angle-dependent macroscopic scattering cross section, $\sigma_s N_A \rho/A$. Note that in the writing of Eq. (14.2), the collision term has been linearized, by assuming that the density of particles in the source beam is low enough to neglect particle-particle collisions in the source, and only collisions with the target atoms and nuclei are considered.

The analytical solution of the Boltzmann equation has been attempted for simple geometries, assuming a monoenergetic source and a homogenous isotropic scattering medium (see e.g.,[17,18]). In any practical case, recourse to numerical methods is necessary to obtain solutions for complex geometries, multi-material targets, and sources with complex energy and momentum spectra. Particle transport is an inherently stochastic problem where all quantities and processes are naturally described by probability distributions. Considering the daunting number of possible interactions that a particle can undergo in the target, and the different type of secondaries that can be generated, the MC family of numerical techniques represent a very convenient solution method. Instead of integrating the probability distributions under given initial and boundary conditions, in the MC method the same distributions are randomly sampled, producing a collection of representative particle "histories" (usually in the figure of many millions), from which physical quantities of interest can be derived by statistical averaging from these distributions. It can be said that MC methods essentially create a statistical sample of a complex problem for which a direct solution is unattainable.

To construct a MC simulation, it is more convenient to put the Boltzmann equation (14.2) in integral form, by performing the integration over the time variable via a conveniently chosen integrating factor. According to the Ergodic Theorem of Birkhoff and Von Neumann [19], the average of a function along the time trajectory is equal to the ensemble average over all phase space, in the limits of infinite time and sample size, respectively. On this basis, one can replace the time variable with a pathlength variable *s* along the direction $\vec{\Omega}$, by defining: $\vec{r}' = \vec{r} - s\,\vec{\Omega}$, which allows to write the translation term as [4, p. 403]:

$$\frac{1}{v}\frac{\partial\psi}{\partial t} + \frac{\partial\psi}{\partial s} + \mu_t\psi(x) = S + q \tag{14.3}$$

where q indicates the scattering (double) integral in the r.h.s. of equation (14.2). A detailed treatment of this equation can be found in the many reviews about particle transport [1–4]. By introducing the integrating factor $\beta = \int_0^s \mu_t sds$, also called optical thickness, the Boltzmann equation turns into:

$$\psi(\vec{r}, E, \vec{\Omega}) = \int_0^\infty ds\, e^{-\beta} \left[S(\vec{r}, E, \vec{\Omega}) + \int_0^{Emax} dE' \int_{4\pi} d\Omega' \mu_s(\vec{r}, E', \vec{\Omega}') \psi(\vec{r}, E', \vec{\Omega}') \right] \qquad (14.4)$$

This form of the equation can be approximated as a series of events, alternating collisions and free flights (Von Neumann series): (i) a particle is started by sampling the source $S(\vec{r}, E, \vec{\Omega})$; (ii) it is transported to a position $\vec{r}$, sampled from the path-length distribution β; (iii) at this site, it makes a collision, and changes its direction and (possibly) its energy to values sampled from the collision kernel, $\mu(\vec{r}, E', \vec{\Omega}')\psi(\vec{r}, E', \vec{\Omega}')$; then it moves to a successive position $\vec{r}'$ as in (ii), where it will make a new collision (iii), and so on, until it is absorbed, or escapes from the system boundaries. This succession of free-flights and collisions (the particle "history") is the essence of the MC algorithm, which can be also explicited in an integral-kernel form, for the sake of mathematical formalism; a detailed treatment of the MC approximation to the Boltzmann equation can be found in the many reviews about particle transport [1–4].

14.3 The Monte Carlo method

As hinted in the previous section, in the MC method particles are transported step-by-step accounting for the stochastic nature of their microscopic interactions. The interactions of individual primary ions and their secondaries are sampled to build a history of charged particle passage and energy deposition in 3-D geometries [4,16]. Depending on the type of incoming radiation and its energy, different interaction processes have to be considered (see Figure 14.1), whose details (energy- and angle-dependent cross sections) are provided by experimental data and/or theoretical models of the elementary interactions.

Each particle individual path is modelled statistically while undergoing the different interaction processes. The final result is calculated by considering a large enough statistical sample of the path (i.e., time-) trajectories to obtain a good approximation of the phase space density, or the particle flux.

At each step of the Von Neumann series, the path length of free flight and the collisional interactions (and their outcomes) follow from a random selection of the corresponding variable from the appropriate probability distributions. Indeed, a key aspect of the MC technique is the ability to generate a sample of phase space points *x* distributed according to a Probability Density Function (PDF) *f(x)* of the *x* variable (*x* can be multidimensional). The samples are (pseudo)random values of a variable distributed according to a PDF that embodies the physics of the interaction, which implies a random sampling of the outcome of physical events from probability distributions.

The "golden rule" of the Monte Carlo method is based on the use of a homogeneous pseudo-random number generator in the interval [0,1], to sample any arbitrary probability density. Starting from the density $f(x)$, a positive quantity defined on some interval $[a,b]$ with integral

normalized to 1, the cumulative density function $F(x) = \int_a^b f(x)dx$ is constructed (CDF). By definition, $F(x)$ is monotonically increasing from 0 to 1 in $[a,b]$; then, a random number $\xi \in [0,1]$ is used to invert the CDF, as $y = [F(\xi)]^{-1}$. By construction, y is an approximant of the functional derivative of the CDF, that is $y \to f(x)$, the original PDF. With this general method, any PDF can be sampled, be it given in analytical, numerical, or tabular form, for any variable in the MC simulation: the pathlength *s,* the scattering angles $\Omega=(\theta,\phi)$, the cross sections for any atomic/nuclear events (elastic scattering, photoelectric, Compton, capture, fission etc.), and so on.

The use of Pseudo Random Numbers (PRN) generator algorithm is needed as computers can not generate true random number sequences. A PRN is a deterministic algorithm that, given the previous state in the sequence, can generate the next number with (almost) no correlation with the preceding one. Such algorithms need a seed to start a sequence and, being deterministic they will always produce the same sequence when initialized with that state. This allows to reproduce the same results when the same code is run on different computers (and it also obviously helps with the debugging of MC codes). For the practical applications of MC codes, very efficient PRN algorithms exists, that can generate very long sequences of uncorrelated numbers (up to 2^{241} or $>10^{70}$ for the most recent PRNs.

14.3.1 Continuous slowing down approximation, condensed history technique and thresholds

The Monte Carlo method can be applied independently on the type and properties of the transported particles. However, there are some important differences when dealing with charged particles, compared to the case of neutral particles. The latter (neutrons, photons) experience occasional interactions with individual target particles (electrons, nuclei) separated by a relatively large free pathlength, giving rise to the characteristic exponential attenuation profile. Instead, when a charged particle passes through a material it actually experiences a huge density of interactions per unit pathlength, both with the nuclear electric field, the mean electron field, and with individual outer shell electrons of the single atoms, because of the long range of the Coulomb field [4]. Therefore, unless the particle velocity falls below a cut-off value roughly corresponding to its de Broglie wavelength, $\lambda=h/mv$, being much larger than the interatomic distances (that is, about $10^{-3}c$ for an electron, or $10^{-6}c$ for a proton), it is normal practice to model the energy loss of charged particles as continuous, with a rate equal to the electronic stopping power, given by the Bethe Bloch equation [20]:

$$-\left(\frac{dE}{dx}\right) = \frac{4\pi\rho Z r_e^2 m_e c^2}{A}\,\frac{z^2}{\beta^2}\left(\ln\frac{2m_e c^2\beta^2\gamma^2}{I^2} - \beta^2 + C - \delta\right) \tag{14.5}$$

with $\beta=v/c$ the particle velocity, $\gamma = (1-\beta^2)^{-1}$ the Lorentz relativistic factor, Z and z the electric charges of the target atom and of the moving particle, ρ the medium density (g/cm^3), I the mean excitation potential of the target atom, and C and δ are to corrections respectively due to excitation close to shell boundaries (relevant for small energies) and a density correction due to polarization, relevant for high energies. The so called Barkas correction [20] is sometimes added, representing a correction due to the electron capture of the positively charged protons at low energies in the domain of the Bragg peak and behind, leading to a slightly increased range of the moving

particle, whereas the negatively charged anti-protons cannot capture electrons from the environmental electrons.

The attenuation coefficient along a pathlength segment *ds* can then be written as the sum of two terms

$$\mu_s\left(\vec{r}, \hat{\Omega} : \hat{\Omega}', E : E'\right) = \frac{d\psi}{dE}\frac{d\mathrm{E}}{ds} + \mu(\hat{\Omega} : \hat{\Omega}') \cdot \delta(E' - E) \tag{14.6}$$

The first term represents the continuous energy loss involving no scattering, while the second term describes the scattering without the energy loss. In this scheme, called *continuous-slowing-down approximation* (CSDA), the particle attenuation is no longer exponential, but has a one-to-one correspondence with the energy loss. The travelled distance is obtained by integrating the reciprocal of the total stopping power over each discrete energy loss ΔE, and the maximum penetration depth (or CSDA range) corresponds to the integral from the initial particle energy E_0 to zero. The CSDA range marks the limit at which all charged particles of a given type with the same energy are absorbed in a given medium. Due to the particular form of the stopping power (14.6), the energy loss increases rapidly with decreasing energy, concentrating the maximum of energy deposition in the target towards the end of the trajectory (the so-called *Bragg peak* of energy deposition).

Notably, assuming the CSDA implies that all particles with the same energy are assumed to travel the same average distance [21]: this is why the CSDA range is a close approximation to the average path length travelled by a charged particle as it slows down to rest. However, in reality particles lose energy in random individual encounters, and their energy after a collision is a continuous distribution, rather than a fixed value: this problem, called *energy straggling*, is more important for lighter than for heavy penetrating particles (typically electrons, which obviously have the same mass of atomic electrons, and therefore can share the kinetic energy in all possible proportions from 0 to E_0). A correction scheme due to L. Landau [22] allows to take into account this energy spreading, in the form of a universal function applied to the distribution of ΔE values, for a given traveled pathlength Δs (see below).

An approximation similar to the CSDA for the energy loss is adopted also for the angular deflection, mostly originating from the elastic scattering, by calculating an average angular distribution (Goudsmit-Saunderson, or Molière approximations [4]) that results from the cumulative effect of a large number of small deflections, along a pathlength segment Δs. The above ensemble of approximations for particle kinetics, common to most MC particle transport codes, makes up the so-called *condensed-history* Monte Carlo method for charged particle transport simulations [16], in which many discrete events are replaced by a straight continuous step, and the corresponding energy losses and changes of direction are condensed into a sum of losses (stopping power) and an overall scattering angle. In a condensed history, a large numbers of interactions along a small segment Δs of the radiation track is accounted via a "cumulative" effect and the typical spatial resolution is of the order of mm.

14.3.2 Computational efficiency and variance reduction techniques

MC calculations results are obtained as the most probable value of a quantity x of interest (e.g., flux, number of created isotopes, energy deposition in a volume, etc.), calculated on the ensemble of particle "histories", indeed a statistical sample of the actual transport problem. Given the finite size of the statistical sample, such "results" are extracted from a suitable average of the quantity of interest, over the set of samples. By their very nature, MC methods suffer from statistical uncertainty, or variance, due to finite sampling. According to the central limit theorem, the uncertainty is inversely proportional to the square root of the number of independent samples (this is strictly true for Gaussian statistics, and in practice this is the case for an unbiased sample). Thus, for each particle, for each desired quantity, averages can be computed as well as their standard deviation σ:

$$\bar{x} = \frac{1}{N}\sum_{n=0}^{N} x_{\mathrm{n}} \quad , \quad \sigma(x) = \sqrt{\frac{1}{N-1}\sum_{n=0}^{N}(x_{\mathrm{n}} - x_0)^2} \tag{14.7}$$

with x_n being the contribution of the n_{th} element in the sample (one particle "history").

Several techniques of biased sampling must be used in practical applications, in order to reduce the variance (for a given amount of computing time) and accelerate convergence (to reduce the overall computing time). The general approach is to modify the PDF corresponding to some interaction event, in order to artificially increase or decrease the corresponding probability in a controlled way, while taking into account the effect of the biasing by a numerical correction factor. Such methods go under the general name of "variance reduction techniques", in the following we give some details of the most important ones.

Modified collision density. Since the number of events necessary to achieve a given statistical precision may be very high, it is sometimes necessary to artificially increase the number of collision events in specific zones. Such approach is often necessary for neutral particles, which may experience rare collisions in a small volume, or in a low-density medium. Collisions can be "forced" by locally increasing the value of a cross section; to compensate for the artificial increase, the score (energy deposition, particle absorption, etc.) is reduced by a factor ("weight") inversely proportional to the biased cross section. This goes also under the name of pathlength stretching, since the distance to the next collision is given by the exponential of the cross section. The notion of particle weight is generally useful in a MC method, as a multiplicative factor that relates to the importance of an event. Particles can carry a weight larger or smaller than 1 (the unbiased value) and their contribution to any event is weighted by this factor.

Range cut-off. If secondary charged particles have a residual range (that is, the integral of $(dE/dx)^{-1}$ from the current value of energy to zero) insufficient to reach the volume of interest, they are suppressed by releasing their residual energy on the spot. Alternatively, the pathlength step time can be adjusted, by adopting the best value in each zone.

Adjusted energy thresholds. Transport and production thresholds are helpful for reducing computer time, but also are needed because of limitations in the validity of the physics model used to describe the cross sections of the different processes. Production energy thresholds are needed for explicit production of Bremsstrahlung radiation (below such a threshold, the electron radiative energy loss is included in the stopping power, dE/dx), or for the explicit production of

secondaries by photons and electrons. A δ-ray threshold sets the limit between discrete and continuous ionization energy losses. Transport thresholds are such that the transport of a particle is stopped when its energy is lower than the preset threshold; in this case, its remaining energy is deposited at that point, or better, in the case of a charged particle, is distributed along its residual range [16].

14.3.3 Some (other) approximations

To conclude this brief introduction to the technical aspects of MC methods in particle transport, it may be relevant to discuss some of the underlying assumptions and approximations that are common to most MC transport codes.

Firstly, the transport of particles is described as a *Markovian process*: after each time interval during which the distribution of the phase-space points migrates from one cell to another one, all the correlations are destroyed. This means there are no memory effects, i.e. the fate of a particle depends only on its actual present properties, and not on previous events or histories. This is a valid assumption if the characteristic times of the fluctuations (the scattering processes) in each phase-space cell are very little with respect to the characteristic times of the distribution evolution (the transport processes) [4]. While this assumption does not seem to present particular problems, the additional assumption that particles do not interact with each other is not valid in extremely intense radiation fields.

Target materials are assumed to be amorphous, that is the macroscopic interaction cross sections are obtained by a simple stoichiometric averaging of the elemental cross sections. This is a reasonable approximation for macroscopic conditions, but effects like channelling of ions within crystallographic planes is starting to be considered in new implementations of MC codes for high energy [23]**.** In almost all applications, materials are considered as continuous, homogeneous and isotropic. For the important problem of transport of cosmic rays in the atmosphere of planets, which would require a description of the variable density and temperature of the atmosphere, MC codes usually approximate the continuous density variation by many discrete layers of uniform density [24]. Furthermore, materials are static: there is no dynamics induced in them by the impact of primaries and the generation and passage of secondaries.

The accuracy of MC calculations does not depend only on the number of particle histories, with statistical convergence possibly accelerated by biasing, but also on the models or data on which the probability distribution functions are based. It has actually been shown that deficiency in the accuracy or in the knowledge of the fundamental light fragment and neutron production cross sections is critical, in particular for the study of galactic cosmic rays transmission through matter (shielding, spacecraft components, and human tissue) [25].

The CSDA previously mentioned continuous uses as input the electron stopping power of the projectile in the material being considered. The CSDA implies a one-to-one correspondence between the particle energy and the travelled distance at each step. However, energy loss has a statistical nature, which means that actually the probability of losing an energy in a certain range ΔE around E, when travelling for a certain path-length, should be considered. The fluctuations around a mean value of the energy loss (straggling) are described by a distribution that is sampled within the transport operator as an energy-dependent step function used to boost the energy loss

by quantities $d\Delta E$ with probability $p(\Delta E, s)$, with respect to the continuously decreasing energy loss from the transport operator [4]. As a matter of fact, without an appropriate correction, the CSDA overestimates the effective projected ranges, because of the range straggling of charged particles, especially at low energies where nuclear collisions and multiple scattering become dominant. For high energy ions, on the contrary, the effective stopping power is the same as the CSDA stopping power, because the loss of energy is mainly by collisions with the atomic electrons and by nuclear interactions.

14.3.4 Geant4 and the suite of applications for space studies

An overview of several MC particle transport codes currently in use in the scientific community is provided in Table 14.1. Among these, the Geant4 code [26] is especially well-designed to simulate high-energy processes with nearly any kind of particle as source. The software suite, with the source code written in C++, is freely available. Geant4 is not a unique code, but a set of libraries which can be used to build specific applications. The user can modify and combine any parts of the code according to the requirements of each particular system to be simulated (https://geant4.web.cern.ch/support/user_documentation). Other widely used codes, such as MCNP6 [27], FLUKA [28], HETC-HEDS [29] and SHIELD [30] do not seem to be as flexible as GEANT4. MCNP6 also requires a license and is a trademark of Los Alamos National Security (LLC, Los Alamos National Laboratory); FLUKA (a code mostly devoted to high-energy physics) requires development to be done in FORTRAN 77, which excludes many features available using more modern programming languages (although only partly true, as routines can be added in F95 and later cross-linked). While PHITS [31], MCNP [27] and GEANT4 [26] support multithreading and Message Passing Interface (MPI), thus being adapted to massively-parallel computing environment, the other codes require splitting large simulations into smaller runs with different random number seeds, and merging the results at the end.

Table 14.1. Comparison of MC codes, particularly used for applications related to space missions

Code/ Developers	Particles transported	Maximum energy	Language/Threading
MNCP Los Alamos National Lab, USA	p,n,μ,γ,π and HZE ions	100 GeV	Fortran/MPI and OpenMP
Geant4 CERN and Geant4 collaboration	p,n,μ,γ,π and HZE ions and other subatomic particles	Over 1 PeV	C++, POSIX Threading, MPI and TOPC
FLUKA INFN and CERN, Italy	61 particles and γ	1 GeV	Fortran/Sequential
PHITS JAEA, Japan	*p,n,η, nuclei, e- and* γ	200 GeV	Fortran/OpenMP
SHIELD JINR and NIR, Russia	any (A,Z) nuclei, *p,n,* π*, K, antinucleons and* μ	1 TeV	Fortran/Sequential
HETSC-HEDS Oak Ridge National Lab and NASA, USA	p,n,μ,γ,π and HZE ions		Fortran/Sequential

A large set of physics "lists" (collection of models/available data for interactions over different energy ranges) is included in Geant4. Such lists have to be combined in order to cover a wide energy range, and even if not the case, to describe the interactions of different charged particles and neutral particles. There exist a very large developer and user communities for this code, which strongly contribute to the further improvement of the physics lists.

In studies of radiation effects induced on both biological and spacecraft components during a space mission, Geant4 is rarely used as standalone tool. A suite of programs and frameworks are used that operate on top of the various Geant4 modules. Examples are the MUlti-LAyered Shielding SImulation Software (MULASSIS), a Monte Carlo-based space radiation analysis tool for use with simple 1-D geometries [32]; the Geant4 Radiation Shielding tool (GRAS) a fully 3-D, MC-based radiation analysis tool tailored for use in space radiation [33]; and more-general frameworks on top of several Geant4 modules, also allowing to obtain the radiation spectra during a space mission, like the SPENVIS online system [34], developed by ESA. Once the energy spectrum of source particles is determined, it can then be used to calculate the effect of interest for the user. Some of these quantities are:

- the degradation of the output current in spacecraft solar cells linked to atomic displacements;
- the absorbed dose in water (see Paragraph 14.2.2), used as proxy for biological tissue reactions in humans, which appropriately scaled can allow to predict the increase of the likelihood for an astronaut to develop cancer [11] and induced short-term effects (cataracts, acute radiation sickness, …) [35];
- the Total Ionising Dose, an important parameter for electronic components and material degradation over the duration of a space mission;
- the so-called Single-Event Effects in microelectronics, causing failure of circuits and sometimes loss of instruments [36].

14.3.5 MC track structure codes

The study of biological effects of ionizing radiation at the cellular level is very important both in the field of ion-beam cancer therapy and in the science that aims at developing more reliable risk assessment models for astronauts and future explorers on the Moon and Mars. The effects at cellular level are strongly linked to the details of the spatial pattern of the energy deposition at the nanoscale induced (mostly) by ionizations ("ionization clusters") within subcellular structures (e.g., DNA, proteins, cell membrane). At such spatial scale, the transport of low-energy radiation becomes a critical component of any quantitative analysis of radiation effects [37], as the penetration of such radiation in matter becomes comparable to the target dimensions (less than 1 μm). Evidence has accumulated through the years that the most important damage to biological molecules is due to secondary electrons with energy around 100 eV (the ionization peak of liquid water and DNA nucleotides) and much below, even <20 eV [38,39,40].

In standard, condensed history MC dosimetric calculations, where the elementary steps Δs represent track segments that are sufficiently long compared to the electron mean free path, and thus group a considerable number of similar collisions, electrons below 1 keV are actually considered to be absorbed on the spot and thus are not tracked anymore below such energy. While

such an approach makes the MC simulation of charged particle transport computationally feasible up to very high energies (MeV-GeV), it is not appropriate to describe the interactions of low energy radiation, as for the latter a resolution down to the nm scale is necessary.

Microdosimetry and nanodosimetry allow, respectively, for a quantitative description of the stochastic aspects of energy deposition in irradiated media at the μm scale and for a quantitative description of key quantities at the nm scale that show connection to the probability of double strand breaks in DNA, such as the distribution of the size of the ionization clusters produced both along the core of the track of the primary particle and in the region affected by secondary electrons (the penumbra) [42]. For very-low-energy electrons, the MC simulation of individual interactions down to ~10 eV energies (event-by-event tracking) can be performed by the explicit calculation of the *track structure*: in practice, this is a step-by-step MC method where electrons are followed in their succession of individual collisions and free flights, with the input of the appropriate electron-electron cross sections (shell ionization, electronic excitation, elastic scattering, etc). The description in the condensed-history approach is clearly not appropriate for resolving the events at very low energies and dimensions, if one is interested in the distribution of clusters of ionization events at the scale of DNA or proteins (a few nanometers) (see Figure 7.4 for the difference between the condensed history and the track structure approach).

A whole family of MC track structure codes has appeared in the past years, like PARTRAC [43], KURBUC [44], RETRACKS (RITRACKS) [45], Geant4-DNA [46] and NOREC [47], today considered the state-of-the-art for nanoscale electron transport; among these, Geant4-DNA is the only open-source code. Most models consider that electrons stop propagating below ~10 eV energy. Notably, the high-degree of detail in track structure models makes the development of the algorithms highly complex, therefore such models are commonly tailored to the single target water, as representative of biological tissues (also considering that a large part of the biological damage to DNA and proteins comes indirectly, from free radicals produced by water radiolysis). The cross sections are derived from semi-empirical linear response theory-based models which make use of the first Born approximation and extrapolate the experimentally available data of the energy loss function at $\vec{q}=0$ to $\vec{q}\neq 0$, where $\vec{q}$ is the momentum of the perturbation [37].

Recent studies have reported a potentially relevant effect of the different models used for the dielectric function of water on ionization clustering [48] and DNA damage induction [49]. Also, there is a high degree of uncertainty as the low energy range cross sections become sensitive to the details of the electronic structure of the target [50]. Recent works have started to implement more realistic targets in Geant4-DNA [51].

14.4 Examples of applications of Monte Carlo particle transport and synergies with quantum dynamics in the electromagnetic sector

In MC codes, the wide coverage of physics comes from a mixture of experimentally available data or modelled cross sections from parametrized models. Each cross-section table or physics model has its own applicable energy range. Combining more than one tables/models, one physics process can have enough coverage of energy range for a wide variety of simulation applications.

Here below we will present some applications which deal with particles of an initially high energy and which allow us to highlight a possible synergy with the approaches in the condensed matter/chemical physics community when particles get slowed down in passing through the target and quantities can be sensitive to the many body physics of the target. Indeed, for low energy interactions, accurate modelling of electronic stopping for ions from real time TDDFT, of defects creation by ab-initio MD and of collisional cascades induced by scattering among nuclei by injecting electronic stopping from real time TDDFT into MD cascades simulations, can well provide better input to MC codes or refine the output from the latter. We will focus on applications on materials of use in Space missions, water and ice targets in astrobiology and radiobiology.

14.4.1 Electronic excitations and atomic displacements in solar cells for space missions

As seen in previous paragraphs, atomic displacements are created by both elastic Coulomb interactions (described by the concept of nuclear stopping) and nuclear (inelastic and elastic) collisions. The resulting structural defects evolve in time, some eventually healing while others leaving defective structures in the system. The solar cells of spacecraft are affected by such displacements, mostly induced by the accumulated impact of the radiation trapped in the Van Allen belts in Earth's vicinity during repeated orbits, and eventually by Solar Energetic Particles (SEPs) events either in Earth vicinity, or in deep Space or on airless bodies like the Moon (not protected by any atmosphere which could eventually attenuate the incoming radiation). The induced cumulative structural defects cause trapping of the charge carriers, degrading the output current. The so-called Non-Ionizing Energy Loss (NIEL) model, which calculates the energy imparted to atomic displacements, is generally used by the radiation-effects community in the field of Space mission design for the prediction and study of the degradation of the performance of the solar cells. The NIEL formula is given by

$$-\left(\frac{dE}{d\chi}\right)_{\text{NIEL}} = \frac{N}{A}\int_{Td}^{E_R^{max}} E_R L(E_R)\frac{d\sigma(E,E_R)}{dE_R}dE_R \tag{14.8}$$

where $\chi = x\rho_A$, with ρ_A being the absorber density in g/cm^3, x the penetration depth of the particle in the material, and N the Avogadro's number, A is the atomic mass of an atom in the material, and E is the kinetic energy of the incident particle. The integration is done over all possible recoil energies E_R between the threshold displacement threshold T_d, the minimum recoil kinetic energy to create a stable defect averaged over all crystallographic directions, and the maximum energy transferred to the recoil nucleus E_R^{max} . $L(E_R)$ is the Lindhard partition function [52] which gives the fraction of the stopping power that goes to NIEL and $d\sigma(E;E_R)/dE_R$ is the elastic Coulomb scattering differential cross section for protons (or other incoming particles) on nuclei. The NIEL generally correlates well with the degradation of semiconductors induced by displacement damage [53]. In several cases there is a linear relationship between the NIEL and the number of displacements when using the modified Kinchin Pease model (Norgett, Robinson and Torrens – NRT – model [54]), based on the BCA (successive independent two-body collisions) for calculations, which partially takes into account a modified efficiency for displacements due to the electronic excitations compared to the hard sphere-model. Such a linear relationship means that indeed the efficiency of producing electrically active defects is a function of the NIEL, and that the damage only depends on the number of defects introduced and not on their variety.

Most of the damage to solar cells in Space comes from protons <10 MeV [55]. For this low energy regime (from few keV to some MeV), Geant4 [26], SR-NIEL [56] or other Geant4-based tools used for space radiation-induced effects use similar assumptions for the Coulomb contribution to the NIEL. In particular, for the energy loss to electronic degrees of freedom, two models are used in all Geant4 electromagnetic physics lists: for protons, for energies below 2 MeV NIST PSTAR/SRIM (TRIM) [57,58] stopping power based on the Lindhard dielectric response theory and above 2 MeV the Bethe-Bloch formula with shell, Barkas, and Bloch and density effect corrections. While the SRIM database is usually assumed to be the accurate reference for stopping power, it is important to note that SRIM electronic stopping values are produced by bringing together a limited number of available experimental results in the form of ratios with respect to He stopping, $r(Z_1, He, v) = S_e(Z_1, Z_2, v)/S_e(He, Z_2, v)$, where Z_1 and Z_2 denote the atomic numbers of projectiles (with velocity v) and target atoms, respectively [59]. For the nuclear stopping, the Ziegler, Biersack, Littmark screened Coulomb potential, fitted among a large set of data [60,61] and the BCA are used. Both the electronic and nuclear stopping power are calculated according to the Bragg's rule, i.e. the (electronic, nuclear) stopping for a compound is obtained as a weighted sum in which each material contributes proportionally to the fraction of its atomic weight. The T_d is a fixed number for each element, independently on the compound in which the element is found. Moreover, the system is considered amorphous and thus channelling effects, where the ions travel in between crystallographic planes, and any dependence of the T_d (the minimum energy to displace an atom and create a stable defect) on the crystalline direction are neglected. In addition, collisional cascades are always considered as adiabatic, e.g. there is no synergy between the electronic and nuclear degrees of freedom, which also means that there is no dependence of the T_d on accompanying electronic excitations produced by the impacting particle or by the recoil atoms.

Deviations from the NIEL scaling hypothesis have been observed, at both high and low energy [62-67]. Microscopic, device-dependent modelling of displacement damage, combining both more sophisticated energy deposition computations and theoretical modelling of the electrical properties of defects and disordered regions is necessary [65,68]. At present, the many approximations done in SRIM are being intensively examined by the condensed matter community [69-73]. Accurate MD calculations [67 and refs. therein] have demonstrated that, in reality, the number of defects can be different from the one described by the NRT model often used in NIEL calculations. Multiscale approaches for radiation damage starting from Geant4 calculations of the produced recoil ions and considering also parameterized approaches for electron and phonon excitations have also been presented [74]. Recent studies show the importance of including electronic stopping effects in cascade formation, in terms of the number of formed defects and cascade morphology [75-83]. The energy transfer from the projectile to the target recoils is a nonionizing event, but the impacting particle and the recoils may deposit locally some energy to the electronic excitations which may alter the formation of defects.

In Figure 14.2 (left panel) we show the results of a MC particle transport calculation performed with the Geant4-based tool MULASSIS for the impact of protons trapped in the Van Allen belts onto a triple-junction solar cells ($Ga_{0.5}In_{0.5}P$/GaAs/Ge) and their passage through the layers of the cell [72], for a 3-year mission in low Earth orbit, with same inclination and altitude of the International Space Station. Taking into account the relative motion between the satellite and the bombarding particles, we can consider that proton and electron irradiation inside the inner Van

Allen belt have an isotropic incidence. The MC calculations show that the range of energies passing through the different layers is essentially as large as the one of the impacting particles, though in such "passing protons" through the layers also protons generated via nuclear reactions are here considered. Nevertheless, many irradiation ground testing experiments are done with unidirectional and monoenergetic 1 MeV proton beams on unshielded solar cells (without the typical protective SiO_2 coverglass), on the basis of previous studies that showed an equivalence between the damage induced in a realistic space environment on shielded solar cells and irradiation of unidirectional monoenergetic protons in ground experiments on unshielded solar cells [62, 85-87]. SRIM results for such unidirectional proton beam (right panel of Figure 14.2) show that 1 MeV protons stop in the Ge bottom layer. As said above, in the calculations of the number of defects via SRIM, which are usually done via the NRT model (in the quick cascade mode, see [73]), the T_d used as input for SRIM is non-direction dependent, is a fixed number for each chemical element, and is not affected by any possible local energy deposition to the electronic degrees of freedom which may influence the displacements.

In Table 14.2 we show the results from ab-initio MD calculations (classical equations of motion for atoms + DFT for electrons) for the T_d for different channeling directions in the Ge layer of the solar cells and, for the PKA in the [110] direction, the different values of the T_d obtained with an ad-hoc consideration of different electronic temperatures (inserted via Fermi-Dirac smearing), reflecting the influence of electronic excitations. The results show that the T_d is indeed different for different crystalline directions, likely influencing the defects that can be created starting from impacting particles or recoils moving in different trajectories, and that the T_d is a dynamical quantity. In Figure 14.3 we show the consequent change in the NIEL curve as calculated from SR-NIEL [56] when considering different values of the T_d (here we have considered the different values corresponding to the different conditions, as these give a higher change in the T_d; curves for the T_d values corresponding to different electronic temperatures would be in the middle between those shown), Clearly, a correct estimation of the T_d has a remarkable impact for proton energies between 0.2 keV and ~8 keV, energies which are surely covered by the protons stopping in the Ge layer under ground testing conditions, and for electron energies between 0.3 MeV and 20 MeV, which surely will pass through the layer. The implementation of the dynamical nature of T_d and of its direction-dependence may be considered respectively in codes such as the recently developed Iradina [88] and the MARLOWE code which allows for crystalline order [89].

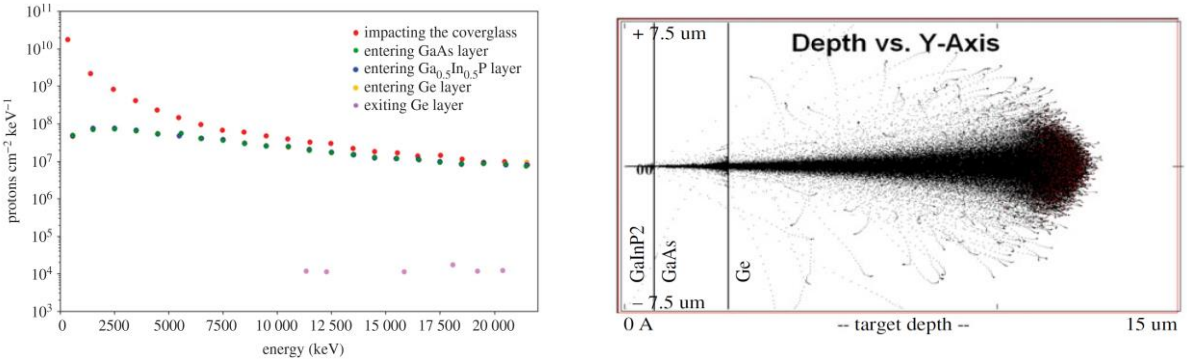

Figure 14.2. Left panel: Fluence of the omnidirectional primary proton radiation across the layers of the solar cell (coverglass included), accumulated during a 3-year International Space Station-like mission, calculated via MC particle transport based on Geant4 (MULASSIS code) [72, 84]. Right panel: ion track trajectory output from TRIM for unidirectional protons of 1 MeV.

Table 14.2. Comparison of threshold diplacement energy value (T_d) obtained from this work and other ab-initio MD results in the literature [90,91], for different channeling directions. In this work, also different values of the electronic temperature Θ_e=1100 K (~0.1 eV), Θ_e=3300 K (~0.3 eV) and Θ_e=4400 K (~0.4 eV) for the PKA along the [110] direction are considered.

Work	Td [111] (eV)	Td[110] (eV)	Td [001] (eV)
[this work]	10	29	18
		27 (Θ_e=1100 K)	
		24 (Θ_e=3300 K)	
		23 (Θ_e=4400 K)	
[90]	9.5	28.5	18
[91]	10.5±0.5	-	18

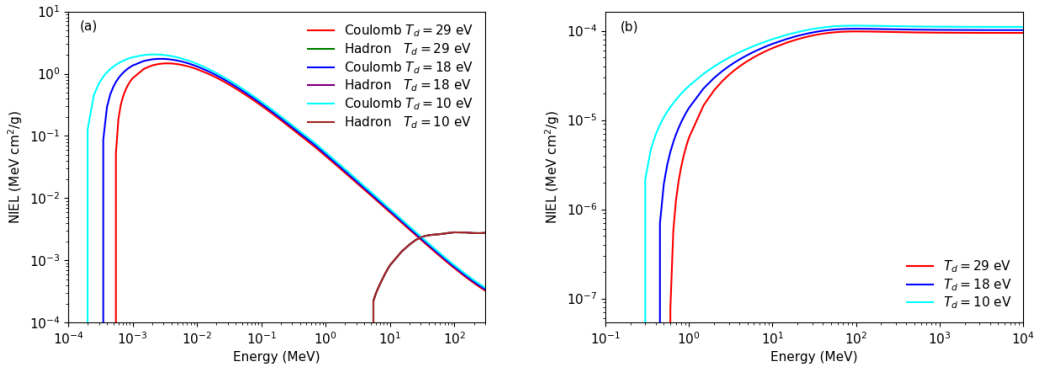

Figure 14.3. a) contributions to the NIEL from both Coulomb interactions and hadron interactions (for protons), and b) from Coulomb interactions (for electrons) for the different T_d in Table 14.2.

14.4.2 Radiation protection in space and astrobiology

There are at least three important possible synergies between the MC particle transport community and the chemical-physics/condensed matter community using ab-initio methods for ion-irradiation studies in the field of radiation protection in space and astrobiology.

MC particle transport codes (in the condensed history approach) are used extensively in studies about the radiation environment and radiation-induced doses around Earth [92], at a spacecraft during possible interplanetary travel missions [93] and around and at the surface of other bodies such as Mars [24,94] and the Moon [95]. The amount of energy deposited by ionizing radiation in the target material (often a water "phantom", considered as a proxy to biological matter) per unit mass is termed the absorbed dose (or simply "dose"), measured in J/kg, or Grays (Gy), is defined as:

$$D(Gy) = \frac{\Delta E}{m} = \frac{1}{\rho} \int_{E0}^{\infty} \frac{d\varepsilon}{dx} f(E) dE \qquad (14.9)$$

where m is the mass of the volume of interest in the target, $d\varepsilon/dx$ is the (unrestricted) collisional stopping power (corresponding to the electronic stopping power, e.g., the energy lost by the particle per unit path length), $f(E)$ is the particle fluence (the flux of particles integrated over the time period of interest), with E being the energy of impacting particles, and ρ is the density in the

volume of interest. The aim of such studies is to estimate the absorbed dose which is then transformed into effective dose, via radiation quality factors which take into account the fact that the same amount of energy deposited in material by two different types of radiation can bring different effects, and thus different levels of risk. The results can then be compared with limits for the effective dose for stochastic effects induced by low doses prolonged in time, such as exposure from the ubiquitous, constant, low flux of Galactic Cosmic rays – GCRs (it must be noted that short term effects induced by high doses, such as those by transient intense events on the Sun, are also of concern).

On the Martian surface, the radiation environment is constituted, under quiet solar conditions, by primary GCRs particles reaching the top of the thin atmosphere and going down without any interaction (apart from ionization), secondaries that are generated via spallation/fragmentation and ionization processes in the planetary atmosphere, and upward secondaries generated by the interactions of the radiation reaching the ground and going below the surface with the regolith of the planet. In particular, Geant4-based calculations (see Figure 14.5), show that the radiation environment as induced by the impact of the GCRs protons and α-particles is mostly constituted by protons ≥ 100 MeV, e^- and γ-particles in the range 1 keV up to 100 MeV, and neutrons spanning a wide energy range down to thermal energies [96].

For most of the energies of the particles reaching the Martian surface, the range of such particles in water (the main constituent of biological matter) is larger than the few nanometers typical of subcellular structures. Thus, dosimetry estimations, at the basis of risk assessment studies for human Mars surface exploration [96] (and at the basis of studies in the astrobiology field, such as those on potential survival of microorganisms, half-lives of eventual biomolecules [97,98], or those on astrophysical ices such as comets in search for organics [99]) are indeed commonly performed on the basis of dose estimations using the MC condensed history approach and the CSDA. For operational radiation protection (measurements and assessment of doses in the body), quality factors, Qs defined as a continuous function of the LET of the radiation (ICRU 2007 [100]) are commonly used.

However, it is now widely accepted by the scientific community that the radiation quality factors are not only related to the (restricted) Linear Energy Transfer (LET, the energy deposited in the system "locally", equal to the electronic stopping power of the particle minus the energy brought away from the volume by high energy secondary electrons), but also to the pattern of energy deposition on the microscopic and nano-scale, the track structure [101,102,103]. It is recognized that particles (of different charge and different speed) with the same LET may show differences in the final biological effects. This is however neglected in specifying Q as a simple function of LET [104]. Microdosimetry, the study of the pattern of the energy deposition at micrometer length scale [105], provides useful insights on a combination of several stochastic processes, including the restricted LET, track length distribution and the energy-loss straggling of the primary particles [106]. Nevertheless, it is now the field of nanodosimetry which is at the basis for the development of new approaches for radiation quality factors. Nanodosimetry provides information on the details of the spatial pattern of energy deposition at the nanometer scale, particularly relevant for the low energy electrons as mentioned in paragraph 14.1.8. A new model has recently been developed at NASA [107] that allows for incorporation of these track structure features in the formulation of new quality factors, which do not only dependent on the LET but also on the charge and velocity of the particle. This is an important conceptual difference between the quality factors

used by NASA for projection of risk from space exposures and the quality factors recommended by the ICRP which only depends on the LET, which are more appropriate for operational radiation protection on Earth. Real time TDDFT modelling could provide information on the spatial pattern of ionization events as induced by particles of different charge and speed, for the low speed regime, the energy range where non perturbative effects appear.

A second important possible synergy comes from the need of MC track structure codes to have as input the cross sections, for both elastic and inelastic processes, for the incoming and secondary particles. The quality of this cross sections obviously influences the accuracy of the final results, and currently this is a main issue especially for the hazardous low energy electrons, but improvements for low energy protons are also needed. The cross sections at low energy and datasets internationally recommended to serve as benchmark for the MC track structure results still have a high level of uncertainty. This is valid in first instance for the hazardous low energy electrons, but improvements for low energy protons are also needed. In this context, an opportunity for synergistic studies with the ab-initio molecular/chemical-physics community is offered by the fact that ab-initio approaches can in principle provide high-accuracy cross sections, the main input needed by MC track structure codes. Such calculations are nowadays done in different flavors, where actually ab-initio techniques are mixed with some semi-empirical modelling to different extents [108-110], although recently an approach has been put forward to extract cross sections from TDDFT calculations in a fully ab-initio manner [111].

Nanodosimetry calculations have also been recently performed for the study of irradiation of astrophysical ices [95]. Recent results from the MC track structure code Geant4-DNA [112] have shown that the radius of a cylindrical volume comprising the trajectories of the primary ion and all secondary electrons, which will collectively determine the effects on an icy target, has a certain dependence on the electronic stopping power. The study of radiation impact on icy targets is not only relevant for astrophysical ices, such as comets or icy grains, but can also be relevant for underground ice on Mars. Protons reaching the subsurface of Mars are slowed down by the interaction with the regolith, and can reach even the keV range, as shown by Geant4 calculations [113,114]. This is relevant as it is likely in the subsurface ice permafrost that we have a chance, if any, to find traces of life, as it has been demonstrated that some microorganisms are able to thrive on environments subject to regular radiation [115] and to survive in a dormant state in icy environments. Thus, improved modelling of the energy loss processes of protons in subsurface ice permafrost is desirable, to answer the question of how much energy can be deposited in such ice layer, what are the effects of the radiation on it at the atomistic scale, and whether we can predict the radiolysis products of the Martian subsurface as these would be potential nutrients of those putative microorganisms. Real time TDDFT calculations can determine very accurately quantities such as the electronic stopping power of protons on an icy sample, shown as a function of the trajectory of the projectile in Figure 14.4. The electronic stopping for 100 keV protons impacting onto ice shows a strong dependence on the impact parameter [116]. This observation is of general importance, for both possibly organic samples trapped in ice and in radiobiology: indeed, since the size of the target volumes considered in nanodosimetry is always smaller than the lateral extension of the penumbra of the primary particle track, the distribution of the clustered ionization events depends critically on the geometrical position of the nanodosimetric target volume with respect to the particle track. The dependence on the impact parameter does indeed affects the hole and excitation populations of the different orbitals [117] (also seen in localized

representations such as the Wannier function picture), which makes it possible to make predictions regarding the radiolysis mechanism of the different chemical species, considered by some authors as a mechanism providing potential availability of nutrients to possible microorganisms [115].

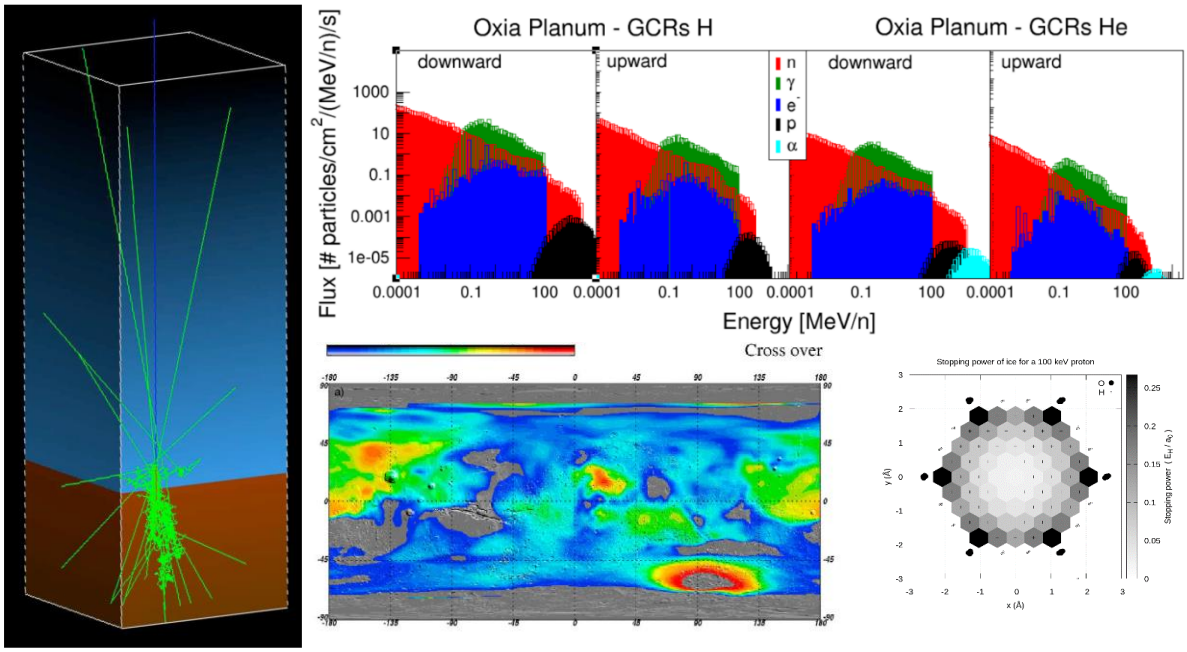

Figure 14.4. Illustration of the geometry used in GEANT4 calculations as a section of 150X150X250 km3. The air shower was initiated by Galactic Cosmic Rays protons and α-particles [96]. Tracks from a low statistic simulation are for a pure illustrative scope [97]. A Map of subsurface ice on Mars [119]. Electronic stopping power for a 100 keV proton impacting on ice, as a function of the impact parameter, from TDDFT calculations combined with Ehrenfest dynamics.

14.4.3 Ion-beam cancer therapy: down to complete stopping

A last example where ab-initio methods based on TDDFT can be of use is the field of ion-beam therapy, where irradiation with light ions is getting increasingly popular compared to traditional photon-based radiotherapy. Such increased use of light ions beams is due to the better confinement of the achieved dose distributions in the region of the tumour and the increased relative biological effectiveness (RBE), the ratio of biological effectiveness of such ionizing radiation relative to X-rays, given the same amount of absorbed energy.

The optimal use of ion radiotherapy heavily relies on modelling. The treatment planning has to account primarily for the distribution of the deposited dose, for a significantly enhanced biological effectiveness of the impacting protons relative to photons at a sub-mm section at the track ends, and also for an accurate estimation of the penetration depth. For real time TDDFT methods, for disordered systems like water, the main component of biological matter, it is still a challenge to obtain a meaningful electronic stopping with a single or few trajectories. Sampling trajectories on a uniform grid, or stochastically generated, require a relatively large number of trajectories for convergence [120]. However, recently, an ion trajectory pre-sampling method has been developed which greatly improve the computational efficiency [121]. This method selects trajectories on a geometric basis, by comparing the probability distribution function (PDF) of the distance between the projectile and the nearest atoms for the supercell to be simulated via RT-TDDFT, with the converged distribution obtained for a large sample. The trajectories are scored according to the

overlap between all sampled trajectories accumulatively and converged distributions for all chemical species present in the target, e.g. H and O for the case of water.

Figure 14.5 left panel depicts the electronic stopping curves as a function of velocity for protons in liquid water, obtained by real time TDDFT calculations, based on Gaussian basis sets, with only 8 pre-sampled short trajectories at the length of 20 Å, and the comparison with available experiments. It can be seen that, with the geometry pre-sampling of ion trajectories, TDDFT calculations can reproduce an accurate electronic stopping (S_e) curve around the Bragg peak for protons in liquid water, with a relatively small demand of computational resources.

An important quantity in radiation therapy is the penetration depth. Protons beams (and in general radiation beams) have a finite penetration depth in a given material. They exhibit a relatively low ionisation density at the surface; their ionisation density increases near the end of the beam range, where there is a narrow region of high ionisation density, i.e. the Bragg peak. The radiation dose from a proton beam falls off sharply both laterally and distally [122], which leads to a limited damage induced in healthy tissues surrounding the tumor. For clinical applications, several beams can be combined to achieve the appropriate dose in the volume of interest, via the superposition of Bragg peaks of different intensities and energies ("spread-out Bragg peak", SOBP). Particles undergo a rapid, non-linear change in their energy deposition characteristics for the end of the range and the increase of LET combined with dose falloff can cause range uncertainties of 1-2 mm [123,124]. Therefore, improved calculations for describing the energy dependence of the RBE down to the stopping limit [125], and removal of the uncertainties regarding the range are critically needed.

In Figure 14.5 right panel we report how the electronic stopping curves around the Bragg peak derived from TDDFT and SRIM affect the penetration range (R). The red line shows the differences of R (ΔR) for protons in liquid water based on the S_e curves of TDDFT and SRIM (red dashed and gray solid lines). The contribution from the nuclear stopping (S_n) of the SRIM tables is also shown as green line. It can be seen that, on the left side of the Bragg peak and below 0.1 MeV, ΔR induced by the difference in Se between TDDFT and SRIM tables is up to 80 nm, as a relative overestimation in Se by TDDFT. For higher energy, the value of ΔR (S_e) decreases to 0 and then goes up in the opposite direction to -11 um at about 2.5 MeV. The negative sign means that the penetration depth given by SRIM table is bigger than that of TDDFT. For proton beams used in therapy, the typical energy is between 50 MeV and 250 MeV with a range over 10 mm [126]. The 11 μm difference due to the difference in S_e between TDDFT and SRIM around the Bragg peak is negligible. In comparison, the contribution from nuclear stopping (ΔR (S_n)) is very tiny around the Bragg peak. It will be increased continuously to about 0.16 mm at 250 MeV (not shown in the figure).

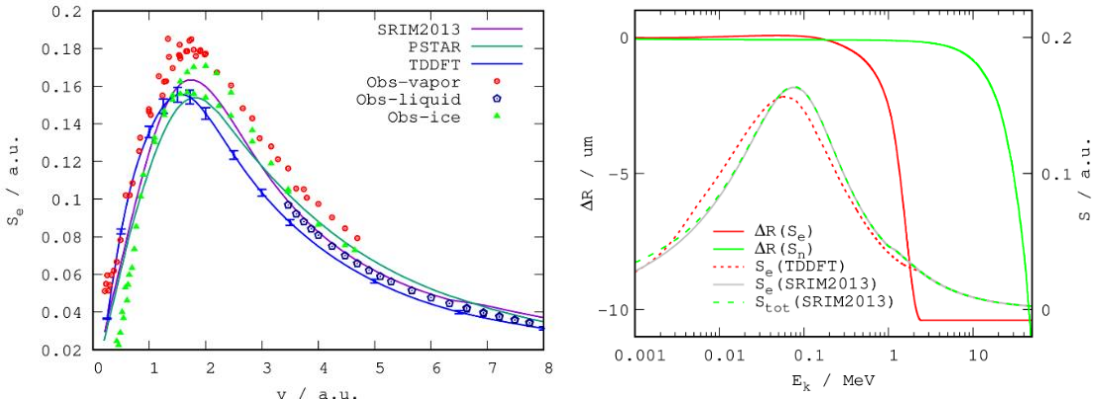

Figure 14.5. Right panel: The purple and dark-green lines show the empirical tables of SRIM2013 and PSTAR, individually. TDDFT calculations,based on Gaussian basis sets, and with 8 pre-sampled short trajectories at the length of 20 Å, are given as blue line with error bars [121]. Available observations of the electronic stopping power for proton in water and ice are also reported, [https://www-nds.iaea.org/stopping/stopping_hydr.html, and references therein]; Left panel: penetration range difference ΔR for proton in liquid water based on the electronic stopping curves of TDDFT and SRIM.

Acknowledgments

This work has received funding from the Research Executive Agency under the EU's Horizon2020 Research and Innovation program ESC2RAD (grant ID 776410). This work benefited from networking activities carried out within the EU funded COST Action CA17126 (TUMIEE) and represents a contribution to it.

References

[1] M. H. Kalos and P. A. Whitlock. Monte Carlo Methods, volume I, Basics. John Wiley & Sons, New York, (1986)

[2] I. Lux and L. Koblinger, Monte Carlo Particle Transport Methods: Neutron and Photon Calculations (CRC Press, 1990)

[3] A. Bielajew, Fundamentals of the Monte Carlo method for neutral and charged particle transport, http://www-personal.engin.umich.edu/~bielajew/MCBook/book.pdf

[4] F. Cleri, Monte-Carlo methods for the study of the diffusion of charged particles through matter, in Proceedings of the IX international School on Nuclear Physics, Neutron Physics And Nuclear Energy, edited by W. Andrejtscheff, D. Elenkov (1990) 401-439

[5] F. Agostini B. F. E. Curchod, R. Vuilleumier, I. Tavernelli and E. K. U. Gross, "TDDFT and Quantum-Classical Dynamics: A Universal Tool Describing the Dynamics of Matter", in Handbook of Materials Modeling : Methods: Theory and Modeling, pp 1-47 (2018) Springer

[6] R. Iftimie, P. Minary and M. E. Tuckerman, Ab initio molecular dynamics: Concepts, recent developments, and future trends, Proc. Nat. Acad. Sci. 102 (19) (2005), 6654-6659

[7] J. Cugnon, Cascade Models and Particle Production: A Comparison. In: Gutbrod H.H., Rafelski J. (eds) Particle Production in Highly Excited Matter. NATO ASI Series (Series B: Physics), vol 303. Springer, Boston, MA (1993) https://doi.org/10.1007/978-1-4615-2940-8_12

[8] D.H. Wright and M.H. Kelsey, The Geant4 Bertini Cascade, Nucl. Instrum. Methods Phys. Res., Sect. A 804. Supplement C (2015) 175 -188

[9] G. Folger, V. Ivanchenko and J.P. Wellisch, The Binary Cascade, The European Physical Journal A - Hadrons and Nuclei 21.3 (2004) 407-417

[10] P. Henrotte. Extension du modèle de cascade intranucléaire pour les réactions de spallation". PhD thesis (2005) Université de Liège

[11] M. Durante and F.A. Cucinotta, Physical basis of radiation protection in space travel, Rev. Mod. Phys. 83 (2011) 1245–1281

[12] J. Benlliure. Spallation Reactions in Applied and Fundamental Research. In: The Euroschool Lectures on Physics with Exotic Beams, Vol. II. Ed. by Jim Al-Khalili and Ernst Roeckl. Berlin, Heidelberg: Springer Berlin Heidelberg (2006) pp 191-238

[13] M. Guthoff, W. de Boer and S. Müller, Simulation of beam induced lattice defects of diamond detectors using FLUKA, Nucl Instr Meth A 735 (2013) 223

[14] J. Miller. Shielding Strategies for Human Space Exploration, chapter Database development and laboratory validation. NASA CP-3360, Langley Research Center, Maryland, USA (1997)

[15] G. Santin. NSREC Short Course notes (2006)

[16] A. Fassò, A. Ferrari and P.R. Sala, Radiation transport calculations and simulations, Radiat Prot Dosimetry 137 (2009) 118-33

[17] V. Boffi and V. Molinari, Solution to the monoenergetic neutron Boltzmann equation for a finite parallelepiped, Transp. Theory Stat. Phys. 1 (1971) 313

[18] V. Kumar and D.C. Sahni, Integral transform method for solving multi-dimensional neutron transport problems with linearly anisotropic scattering, Ann. Nucl. Energy 8 (1981) 173

[19] M.G. Nadkarni, "Ergodic Theorems of Birkhoff and von Neumann" in Basic Ergodic Theory, Texts and Readings in Mathematics 6 (2013). Hindustan Book Agency, Gurgaon. https://doi.org/10.1007/978-93-86279-53-8_2

[20] P. Sigmund, Particle Penetration and Radiation Effects. Springer Series in Solid State Sciences, 151 (2006) Berlin Heidelberg: Springer-Verlag. ISBN 3-540-31713-9

[21] R.E. Johnson, Energetic Charged-Particle Interactions with Atmospheres and Surfaces, Physics and Chemistry in Space No. 19 (1990) Berlin: Springer-Verlag

[22] A, Pedro, and A. Brahme. “Restricted Energy-Loss Straggling and Multiple Scattering of Electrons in Mixed Monte Carlo Procedures.” Radiation Research 100 (1) (1984) 16–29. JSTOR, www.jstor.org/stable/3576517

[23] E. Bagli, M. Asai, .D Brandt, A. Dotti, V. Guidi and D.H. Wright, A model for the interaction of high-energy particles in straight and bent crystals implemented in Geant4, The European Physical Journal C 74 (8) (2014) 1-11

[24] J Guo, TC Slaba, C Zeitlin, RF Wimmer-Schweingruber, FF Badavi, Dependence of the Martian radiation environment on atmospheric depth: Modeling and measurement, Journal of Geophysical Research: Planets 122 (2017), 329-341

[25] D. Matthiä, B. Ehresmann, H. Lohf, J. Köhler, C. Zeitlin, et al, The Martian surface radiation environment – a comparison of models and MSL/RAD measurements. J. Sp. Weather Sp. Clim. 6 (2016) A13

[26] J. Allison, K. Amako; J. Apostolakis; H. Araujo; P. Arce Dubois et al., Geant4 Developments and Applications, IEEE Trans. Nucl. Sci. 53 (2006) 270-278

[27] J. E. Sweezy, T. Booth, F. Brown et al., Mcnp-a general Monte Carlo n-particle transport code, version 5, MCNP user manual, Report LA-UR-03-1987, Los Alamos, CA: Los Alamos National Laboratory, (2003)

[28] G. Battistoni, The FLUKA code, galactic cosmic ray and solar energetic particle events: From fundamental physics to space radiation and commercial aircraft doses, IEEE Nucl. Sci. Symp. Conf. Rec., IEEE (2008) 1609–1615

[29] L. W. Townsend, T. M. Miller and T. A. Gabriel, Hetc radiation transport code development for cosmic ray shielding applications in space, Radiation Protection Dosimetry 116 (2005) 135-139

[30] A. V. Dementyev and N. M. Sobolevsky, Shield — universal Monte Carlo hadron transport code: scope and applications, Radiation Measurements 30 (1999) 553-557

[31] T. Sato, K. Niita, N. Matsuda, S. Hashimoto, Y. Iwamoto et al., Particle and heavy ion transport code system, PHITS, version 2.52, J. Nucl. Sci. Technol. 50 (2013) 913–923

[32] F. Lei, P.R. Truscott, C.S. Dyer, B. Quaghebeur, D. Heynderickx, P. Nieminen, H. Evans, and E. Daly, MULASSIS: A Geant4-Based Multilayered Shielding Simulation Tool. IEEE Trans. Nucl. Sci., 49 (2002) 2788–2793

[33] G. Santin, V. Ivanchenko, H. Evans, P. Nieminen and E. Daly, GRAS: a general-purpose 3-D Modular Simulation tool for space environment effects analysis. IEEE Trans. Nucl. Sci. 52 (2005) 2294 - 2299

[34] D. Heynderickx, B. Quaghebeur, E. Speelman and E. Daly, ESA's Space Environment Information System (SPENVIS) - A WWW interface to models of the space environment and its effects. In 38th Aerospace Sciences Meeting and Exhibit. AIAA (2000)

[35] F.A. Cucinotta,, M. Alp, B. Rowedder and M.-H. Y. Kim, Safe days in space with acceptable uncertainty from space radiation exposure, Life Sciences and Space Research 5 (2015) 31–38

[36] P. Jiggens, M. -A. Chavy-Macdonald, G. Santin, A. Menicucci, H. Evans and A. Hilgers, The magnitude and effects of extreme solar particle events, J. Space Weather Space Clim. 4 (2014) A20

[37] H. Nikjoo, D. Emfietzoglou, T. Liamsuwan, R. Taleei, D. Liljequist and S. Uehara, Radiation track, DNA damage and response: a review, Reports on Progress in Physics 79 (2016) 1166601

[38] E. Alizadeh, T. M. Orlando and L. Sanche, Biomolecular damage induced by ionizing radiation: The direct and indirect effects of low-energy electrons on DNA, Annual Review of Physical Chemistry 66, (2015) 379–398

[39] S. Denifl, T. D. Märk and P. Scheier, "The role of secondary electrons in radiationdamage," in Radiation Damage in Biomolecular Systems, edited by G. García Gómez-Tejedor and M. C. Fuss (2012) pp 45-58, Springer Netherlands, Dordrecht

[40] H. Nikjoo and L. Lindborg, RBE of low energy electrons and photons, Phys. Med. Biol. 55 (2010) R65

[41] I. El Naqa, P. Pater and J. Seuntjens, Monte Carlo role in radiobiological modelling of radiotherapy outcomes, Phys. Med. Biol. 57 (2012) R75–R97

[42] H. Rabus, Nanodosimetry - on the ''tracks'' of biological radiation effectiveness, Z. Med. Phys. 30 (2020) 91-94

[43] M. Dingfelder, R.H. Ritchie, J.E. Turner, W. Friedland, H.G. Paretzke et al., Comparisons of calculations with PARTRAC and NOREC: transport of electrons in liquid water, Radiation research 169, (2008) 584—594

[44] T. Liamsuwan, D. Emfietzoglou, S. Uehara and H. Nikjoo, Microdosimetry of low-energy electrons, Int. J. Rad. Biol. 88 (2012) 899—907

[45] I. Plante and F. A. Cucinotta, Cross sections for the interactions of 1 eV--100 MeV electrons in liquid water and application to Monte-Carlo simulation of HZE radiation tracks, New Journal of Physics 11, (2009) 063047

[46] S. Incerti, I. Kyriakou, M.A. Bernal, M.C. Bordage, Z. Francis, et al., Geant4-DNA example applications for track structure simulations in liquid water: A report from the Geant4-DNA Project, Medical physics 45 (2018) e722--e739

[47] V.A. Semenenko, J.E. Turner and T.B. Borak, TB, NOREC, a Monte Carlo code for simulating electron tracks in liquid water, Radiation and environmental biophysics 42 (2003) 213-2017

[48] C. Villagrasa, M. -C. Bordage, M. Bueno, M. Bug, S. Chiriotti, E. Gargioni, B. Heide, H. Nettelbeck, A. Parisi and H. Rabus, Assessing the contribution of cross-sections to the uncertainty of Monte Carlo calculations in micro- and nanodosimetry, Radiation Protection Dosimetry 183 (2018) 11–16

[49] N. Lampe, M. Karamitros, V. Breton, J. M. C. Brown, I. Kyriakou, D. Sakata, D. Sarramia and S. Incerti, Mechanistic DNA damage simulations in Geant4-DNA part 1: A parameter study in a simplified geometry, Phys. Med. 48 (2018) 135–45

[50] R. Garcia-Molina, I. Abril, I. Kyriakou and D. Emfietzoglou, Inelastic scattering and energy loss of swift electron beams in biologically relevant materials, Surf. Interf. Anal. 49, (2017) 11–17

[51] S. A. Zein, M.-C. Bordage, Z. Francis, G. Macetti, A. Genoni, C.Dal Cappello, dW.-G. Shina and S. Incerti, Electron transport in DNA bases: An extension of the Geant4-DNA Monte Carlo toolkit, Nucl. Instrum. Meth. B 488 (2021) 70-82

[52] M. Scharff, P. V. Thomsen J. Lindhard and V. Nielsen, Integral equations governing radiation effects, Mat. Fys. Medd. Dan. Vid. Selsk., 33 (10) (1963)

[53] C. Inguimbert, P. Arnolda, T. Nuns and G. Rolland, “Effective NIEL” in Silicon: Calculation Using Molecular Dynamics Simulation Results, IEEE Trans. Nucl. Sci. 57 (4) (2010) 1915 - 1923

[54] M.J. Norgett, M.T. Robinson and I.M. Torrens. A proposed method of calculating displacement dose rates, Nuclear Engineering and Design, 33(1) (1975) 50-54

[55] C. Poivey, ESA-CERN–SCC Workshop CERN, May 9-10, 2017 https://indico.cern.ch/event/635099/contributions/2570676/attachments/1456363/2249942/4_Radiation_Effects_and_RHA_ESA_Internal_Course_4_10_May_2017_DD_CP.pdf

[56] http://www.sr-niel.org/

[57] NIST: Introduction of ESTAR, PSTAR, and ASTAR. See http://physics.nist.gov/PhysRefData/Star/Text/intro.html

[58] J.F. Ziegler, M.D. Ziegler and J.P. Biersack, SRIM – The stopping and range of ions in matter, Nucl. Instrum. Meth. B 268 (2010) 1818–1823

[59] K. Wittmaack, Misconceptions impairing the validity of the stopping power tables in the SRIM library and suggestions for doing better in the future. Nucl. Instrum. Meth. B 380 (2016) 57–70

[60] J. F. Ziegler, J. P. Biersack and U. Littmark, The Stopping and Range of Ions in Solids, Volume 1 of The Stopping and Ranges of ions in Matter, edited by J.F. Ziegler, Pergamon Press, 1985;

[61] S.R. Messenger, E. A. Burke, M. A. Xapsos, G. P. Summers, R. J. Walters, I. Jun and T. Jordan, NIEL for Heavy Ions: An Analytical Approach, IEEE Trans. Nucl. Sci. 50 (2003) 1919 - 1923

[62] S.R. Messenger, G. P. Summers, E. A. Burke, R. J. Walters, and M. A. Xapsos, Modeling solar cell degradation in space: A comparison of the NRL displacement damage dose and the JPL equivalent fluence approaches, Prog. Photovolt.: Res. Appl. 9 (2001) 103

[63] S.R. Messenger, E.A. Burke, G.P. Summers, M.A. Xapsos, R.J. Walters, E.M. Jackson and B.D. Weaver, Nonionizing energy loss (NIEL) for heavy ions, IEEE Trans. Nucl. Sci. 46 (1999) 1595-1602

[64] S.R. Messenger, E.A. Burke, G.P. Summers and R.J. Walters, Application of displacement damage dose analysis to low-energy protons on silicon devices, IEEE Trans. Nucl. Sci. 49 (2002) 2690-2694

[65] R.A. Weller, M.H. Mendenhall and D.M. Fleetwood, A screened Coulomb scattering module for displacement damage computations in Geant4, IEEE Trans. Nucl. Sci. 51 (2004) 3669 – 3678

[66] M. Huhtinen, Simulation of non-ionising energy loss and defect formation in silicon, Nucl. Instrum. Meth. A 491 (2003) 194

[67] F. Gao, E. Hernandez-Rivera, D. Huang and P. D. LeVan, Displacement damage and predicted non-ionizing energy loss in GaAs , J. Appl. Phys. 121 (2017) 095104

[68] G. Herrero-Saboya, L. Martin-Samos, A. Jay, A. Hémeryck and N Richard, A comprehensive theoretical picture of E centers in silicon: From optical properties to vacancy-mediated dopant diffusion, J. Appl. Phys. 127 (2020) 085703

[69] P. Sigmund and A. Schinner, Electronic stopping in oxides beyond Bragg additivity, Nucl. Instrum. Meth. B 415 (2018) 110–116

[70] M. Caro, A. A. Correa, E. Artacho and A. Caro, Stopping power beyond the adiabatic approximation, Sci. Rep. 7 (2017) 2618

[71] R. Ullah, E. Artacho and A.A. Correa, Core electrons in the electronic stopping of heavy ions, Phys. Rev. Lett. 121 (2018) 116401

[72] N. Koval, F. Da Pieve and E. Artacho, Ab initio electronic stopping power for protons in Ga0.5In0.5P/GaAs/Ge triple-junction solar cells for space applications, Royal Open Science Society 7 (2020) 200925

[73] W.J. Weber and Y. Zhang, Predicting damage production in monoatomic and multi-elemental targets using stopping and range of ions in matter code: Challenges and recommendations, Curr. Opin. Solid State Mater. Sci. 23 (4) (2019) 100757

[74] M. Raine, A. Jay, N. Richard, V. Goiffon, S. Girard, M. Gaillardin and P. Paillet, Simulation of single particle displacement damage in silicon—Part I: Global approach and primary interaction simulation, IEEE Trans. Nucl. Sci. 64 (2017) 133-40

[75] M. Caro, A. Tamm, A.A. Correa and A. Caro, Role of electrons in collision cascades in solids. I. Dissipative model, Phys. Rev. B 99 (2019) 174301

[76] A. Tamm, M. Caro, A. Caro, and A.A. Correa, Role of electrons in collision cascades in solids. II. Molecular dynamics, Phys. Rev. B 99 (2019) 174302

[77] C.W. Lee, J.A. Stewart, S.M. Foiles, R. Dingreville and A. Schleife, Multi-scale simulations of electron and ion dynamics in self irradiated silicon, Phys. Rev. B 102 (2020) 024107

[78] T. Jarrin, A. Jay, A. Hémeryck and N. Richard, Parametric study of the Two-Temperature Model for Molecular Dynamics simulations of collisions cascades in Si and Ge, Nucl. Instrum. Meth. B 485 (2020) 1-9

[79] M. Toulemonde, W.J. Weber, G. Li, V. Shutthanandan, P. Kluth, T. Yang, Y. Wang and Y. Zhang, Synergy of nuclear and electronic energy losses in ion-irradiation processes: the case of vitreous silicon dioxide, Phys. Rev. B 83 (2011) 054106

[80] W. J. Weber, D.M. Duffy, L. Thomé and Y. Zhang, The role of electronic energy loss in ion beam modification of materials, Curr. Opin. Solid State Mater. Sci. 19 (2015) 1–11

[81] E. Zarkadoula, D.M. Duffy, K. Nordlund, M.A. Seaton, I.T. Todorov, W.J. Weber and K. Trachenko, Electronic effects in high-energy radiation damage in tungsten, J. Phys. Condens. Matter 27 (2015) 135401

[82] M. Backman, F. Djurabekova, O.H. Pakarinen, K. Nordlund, Y. Zhang, M. Toulemonde and W.J. Weber, Cooperative effect of electronic and nuclear stopping on ion irradiation damage in silica, J. Phys. D: Appl. Phys. 45 (2012) 50525

[83] T. Jarrin, J. Teunissen, F. Da Pieve, N. Richard, A. Hémeryck, unpublished

[84] F. Lei, R.R. Truscott, C.S. Dyer, B. Quaghebeur, D. Heynderickx, P. Nieminen, H. Evans and E. Daly, MULASSIS: a Geant4-based multilayered shielding simulation tool, IEEE Trans. Nucl. Sci. 49 (2002) 2788-2793.

[85] G.P. Summers, S.R. Messenger, E.A. Burke, M.A. Xapsos and R.J. Walters, Low energy proton-induced displacement damage in shielded GaAs solar cells in space. Appl. Phys. Lett. 71 (1997) 832-834

[86] G.P. Summers, S.R. Messenger, E.A. Burke, M.A. Xapsos and R.J. Walters, Contribution of low-energy protons to the degradation of shielded GaAs solar cells in space, Prog. Photovolt. Res. Appl. 5 (6) (1997) 407–413

[87] G. Summers, E. Burke, M. Xapsos, C. Dale, P. Marshall and E. Petersen, Displacement damage in GaAs structures, IEEE Trans. Nucl. Sci. 35 (1998) 1221–1226

[88] C. Borschel and C. Ronning, Ion beam irradiation of nano-structures—A 3D Monte Carlo simulation code, Nucl. Instrum. Meth. B 269 (2011) 2133–2138

[89] C.J. Ortiz, A. Souidi, C.S. Becquart, C. Domain and M. Hou, Recent radiation damage studies and developments of the Marlowe code, Radiation Effects and Defects in Solids, 169 (2014) 592-602

[90] M. Jiang, H. Xiao, S. Peng, G. Yang, Z. Liu, L. Qiao and X. Zu, A Theoretical Simulation of the Radiation Responses of Si, Ge, and Si/Ge Superlattice to Low-Energy Irradiation, Nanoscale Res. Lett. 13 (2018) 133

[91] E. Holmström, K. Nordlund and A. Kuronen, Threshold defect production in germanium determined by density functional theory molecular dynamics simulations, Phys. Scr. 81 (2010) 035601

[92] T. Ersmark, P. Carlson, E. Daly, C. Fuglesang, I. Gudowska, B. Lund-Jensen, P. Nieminen, M. Pearce and G. Santin, Geant4 Monte Carlo Simulations of the Galactic Cosmic Ray Radiation Environment On-Board the International Space Station/Columbus, IEEE Trans. Nucl. Sci. 54 (2007) 1854-1862

[93] C.J. Mertens and T.C. Slaba, Characterization of solar energetic particle radiation dose to astronaut crew on deep-space exploration missions, Space Weather 14 (2019) 1650-1658

[94] D. Matthiä, D.M. Hassler, W. de Wet, B. Ehresmann, A. Firan, et al., The radiation environment on the surface of Mars-Summary of model calculations and comparison to RAD data, Life Sciences in Space Research 14 (2017) 18-28

[95] G. Reitz, T. Berger and D. Matthiä, Radiation exposure in the Moon environment, Planetary and Space Science 74 (2012) 78-83

[96] F. Da Pieve, G. Gronoff, J. Guo, C.J. Mertens, L Neary, B. Gu, N.E. Koval, J. Kohanoff, A.C. Vandaele and F. Cleri, Radiation environment and doses on Mars at Oxia Planum and Mawrth Vallis: support for exploration at sites with high biosignature preservation potential, J. Geophys Res.: Planets 126 (2021) e2020JE006488

[97] L. R. Dartnell, L. Desorgher, J.M. Ward, and A. J. Coates, Martian sub-surface ionising radiation: biosignatures and geology, Biogeosciences, 4 (2007) 545–558

[98] A. A. Pavlov, G. Vasilyev, V. M. Ostryakov, A. K. Pavlov and P. Mahaffy, Degradation of the organic molecules in the shallow subsurface of Mars due to irradiation by cosmic rays, Geophys. Res. Lett. 39, (2012) L13202

[99] G. Gronoff, R. Maggiolo, G. Cessateur, W. B. Moore, V. Airapetian, J. De Keyser, F. Dhooghe, A. Gibbons, H. Gunell and C. J. Mertens, The Effect of Cosmic Rays on Cometary Nuclei. I. Dose Deposition, The Astrophysical Journal 890 (2020)

[100] ICRP (103) (2007). The 2007 Recommendations of the International Commission on Radiological Protection. Annals of the ICRP, Publication 103. The International Commission on Radiological Protection

[101] H. Nikjoo, S. Uehara, W. E. Wilson, M. Hosh and D. T. Goodhead, Track structure in radiation biology: theory and applications, Int. J. Rad. Biol., 73 (1998) 355-364

[102] H Rabus. Nanodosimetry - on the "tracks" of biological radiation effectiveness. Z Med Phys., 30 (2020) 91-94

[103] T. Friedrich, K. Ilicic, C. Greubel, S. Girst, J. Reindl, M. Sammer, B. Schwarz, C. Siebenwirth, D. W. M. Walsh, T. E. Schmid, M. Scholz and G. Dollinger, DNA damage interactions on both nanometer and micrometer scale determine overall cellular damage, Sci. Rep. 8 (2018) 16063

[104] D.T. Goodhead. Track structure and the quality factor for space radiation cancer risk (reid). Technical report (2018) https://three.jsc.nasa.gov/articles/Track_QF_Goodhead.pdf

[105] H.H. Rossi and M. Zaider. "Microdosimetry and its applications" London, UK (1996) Springer

[106] H.G. Menzel, The complexity of quantities in radiation dosimetry: the issue of radiation quality, Radiat. Prot. Dosimetry 183 (2019) 3-10

[107] F.A. Cucinotta, Review of NASA approach to space radiation risk assessments for mars exploration, Health Physics, 108 (2015) 131-42

[108] M. U. Bug, W. Yong Baek, H. Rabus, C. Villagrasa, S. Meylan and A. B. Rosenfeld, An electron-impact cross section data set (10 eV–1k eV) of DNA constituents based on consistent experimental data: A requisite for Monte Carlo simulations, Rad. Phys. Chem. 130 (2017) 459-479

[109] J.R. Madsen and G. Akabani, Low-energy cross-section calculations of single molecules by electron impact: a classical Monte Carlo transport approach with quantum mechanical description, Phys. Med. Biol. 59 (2014) 2285-305

[110] S. Taioli, P. E. Trevisanutto, P. de Vera, S. Simonucci, I. Abril, R. Garcia-Molina and M. Dapor, Relative Role of Physical Mechanisms on Complex Biodamage Induced by Carbon Irradiation, Phys. Chem. Lett. 12 (2021) 487–493

[111] N. Koval, P. Koval, F. Da Pieve, J. Kohanoff, E. Artacho, D. Emfietzoglou, unpublished

[112] C. N. Shingledecker, S. Incerti, A. Ivlev, D. Emfietzoglou, I. Kyriakou, A. Vasyunin, and P. Caselli, Cosmic-Ray Tracks in Astrophysical Ices: Modeling with the Geant4-DNA Monte Carlo Toolkit, The Astrophysical Journal 904 (2020) 189

[113] L. Röstel, J. Guo, S. Banjac, R.F. Wimmer-Schweingruber and B. Heber, Subsurface Radiation Environment of Mars and Its Implication for Shielding Protection of Future Habitats, J. Geophys Res.: Planets 125 (2020), e2019JE006246

[114] P. M. Silva de Magalhães, Radiation environment and its effects on the Martian surface and underground, Master Thesis (2016) University of Lisbon Técnico Lisboa

[115] D. Atri, On the possibility of galactic cosmic ray-induced radiolysis-powered life in subsurface environments in the Universe, Journal Royal Society Interface 13 (2016) 20160459

[116] D. Muñoz-Santiburcio and E. Artacho, unpublished

[117] K. G. Reeves and Y. Kanai, Electronic Excitation Dynamics in Liquid Water under Proton Irradiation, Sci Rep. 7: 40379 (2017)

[119] W. C. Feldman, A. Pathare, S. Maurice, T. H. Prettyman, D. J. Lawrence, R. E. Milliken and B. J. Travis, Mars Odyssey neutron data: 2. Search for buried excess water ice deposits at nonpolar latitudes on Mars, J. Geophys Res.: Planets 116 (2011) E11009

[120] A. A. Correa, Calculating electronic stopping power in materials from first principles. Computational Materials Science 150 (2018) 291

[121] B. Gu, B. Cunningham D. Muñoz-Santiburcio, F. Da Pieve, E. Artacho and J. Kohanoff, Efficient calculation of electronic stopping in disordered systems: application to liquid water, J. Chem. Phys. 153 (2020) 034113

[122] J. Chen, Microdosimetric characteristics of proton beams from 50 keV to 200 MeV, Radiation Protection Dosimetry 143 (2010) 436-439

[123] L. Paganetti, M. Gerweck and H. Goitein, The general relation between tissue response to x-radiation (α/β values) and the relative biological effectiveness (RBE) of protons: prediction by the Katz track-structure model, Int. J. Rad. Biol. 76 (2000) 985-998

[124] J.A. Lomax, Myths and realities of range uncertainty, British J Radiol. 93 (2011) 582

[125] W. Friedland, E. Schmitt, P. Kundrát, M. Dingfelder, G. Baiocco, S. Barbieri and A. Ottolenghi, Comprehensive track-structure based evaluation of DNA damage by light ions from radiotherapy-relevant energies down to stopping, Sci. Rep. 7 (2017) 45161

[126] W. D. Newhauser and R. Zhang, The physics of proton therapy, Phys. Med. Biol., 60 (2015) R155